Supplementary Material

Biomass burning at Cape Grim: exploring photochemistry using multi-scale modelling

S. J. Lawson, M. Cope, S. Lee, I.E. Galbally, Z. Ristovski and M.D. Keywood

ACP-2016-932

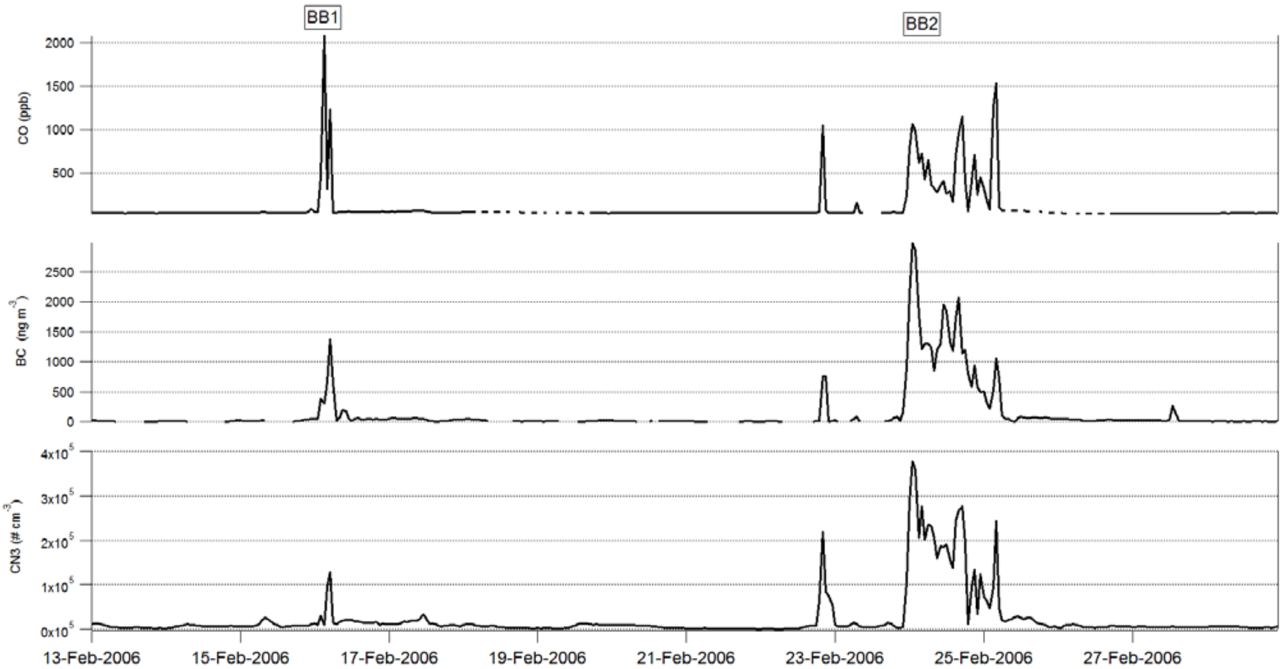

Figure 1. Time series of observed carbon monoxide (CO)- top, black carbon (BC)-middle and particles >3 nm (CN3)-bottom, for the study period. Taken from Lawson et al., 2015.

Performance of the numerical meteorological modelling

The TAPM (Hurley, 2008) and CCAM (McGregor and Dix, 2008) meteorological simulations form an integral component of the analysis presented in our paper. As such, it is helpful to undertake qualitative and quantitative comparisons of modelled and observed meteorological parameters in order to assess the relative performance of each model. Although a full assessment of the performance of TAPM and CCAM were beyond the scope of this project (and not supported by a comprehensive set of observational data), we are able to assess model performance for hourly wind, temperature and humidity which were observed at the Cape Grim Base Line monitoring station. The results of a comparison of these data with the simulations of TAPM and CCAM for the period 13–27 February 2006 are summarised below.

Figure 2 shows the scatter plots of observed and modelled wind, temperature and relative humidity and suggest that TAPM performs marginally than CCAM for the 10 m wind speed modelling with a higher coefficient of determination, a better intercept for the least squares regression line of best fit although a 5% lower slope. CCAM has better performance for the modelling of the screen temperature (significantly better slope and intercept), and TAPM performs better for the modelling of relative humidity (note that this parameter also includes the effect of temperature).

Figure 3 shows the sample probability density functions (pdf) for the observation and model wind speed, wind direction, temperature and relative humidity time series. Note that the observed pdfs differ slightly between the TAPM and the CCAM plots because TAPM times are in Australian Eastern Standard while the CCAM plots are in UTC and the sampling periods are slightly different. In the following we consider the qualitative similarities and differences between the observed and modelled pdfs.

Figure 3 (top row) shows that CCAM has better matched the wind speed pdf, with a good representation of the mode at around 9 ms^{-1}. On the other hand TAPM mode occurs at 7 m s^{-1}. Both models simulate a mode in the wind direction pdf for the sector centred on 75^{o} south (observed mode at 90^{o} south. TAPM successfully models two modes in the west–south-west sector while CCAM simulates a single mode only (at 225^{o}). With respect to the screen temperature Figure 2 (third row) shows that CCAM has better simulated the width and peak of the observed temperature pdf, with TAPM under predicting the pdf width and over predicting the peak.

TAPM does a better job of modelling the RH pdf with CCAM under estimating the width of the pdf and overestimating the magnitude of the mode at 90% RH (Figure 3- bottom).

We complete this section by considering a suite of statistical measures of model performance. Figure 4 shows 10 statistical measures- see Hurley et al. (2005), with more details of the metrics given in Willmott (1981) and Thorpe (1985) which can be used to give a quantitative comparison of the TAPM and CCAM 10 m wind speed simulations. Figure 4 (top row) shows that CCAM simulates the campaign mean wind speed to within -14% (thus a low bias) while TAPM has a low bias of 25%. The observed standard deviation of the wind speed is modelled to within -14% by TAPM and 3% by CCAM- see SKILLv in Figure 4 (bottom row). The root mean square error (RMSE) is 2.5 m^{-1} for TAPM and 3.7 m s^{-1} for CCAM. In this regard, a useful measure of skill is the ratio of the RMSE to the observed standard deviation (SKILLr in Figure 4) with SKILLr < 1 being desirable. It can be seen that both models have satisfied this criteria and that TAPM has performed better than CCAM with respect to this metric. Consideration of the RMSE metrics also indicate general good skill from both models, and with TAPM performing better than CCAM. The Index of Agreement (IOA; unity is ideal) also provides evidence of good model performance.

Figure 5 shows the same statistical measures for screen temperature and again indicates skill in the modelling according to the metrics of Willmott (1981) and Thorpe (1985). Again the TAPM performance is slightly better than CCAM. Similar conclusions can be drawn with respect to the relative humidity (Figure 6).

In summary, a necessary condition is that the meteorological models are able to demonstrate reasonable skill in modelling the meteorological conditions within the vicinity of the smoke trajectories as they couple Cape Grim with the smoke source area on Robbin’s Island. The information presented above is promising (although not a complete model verification), and does suggest that the TAPM simulations are slightly better than the CCAM simulations with respect to the low level wind, temperatures and relative humidity.

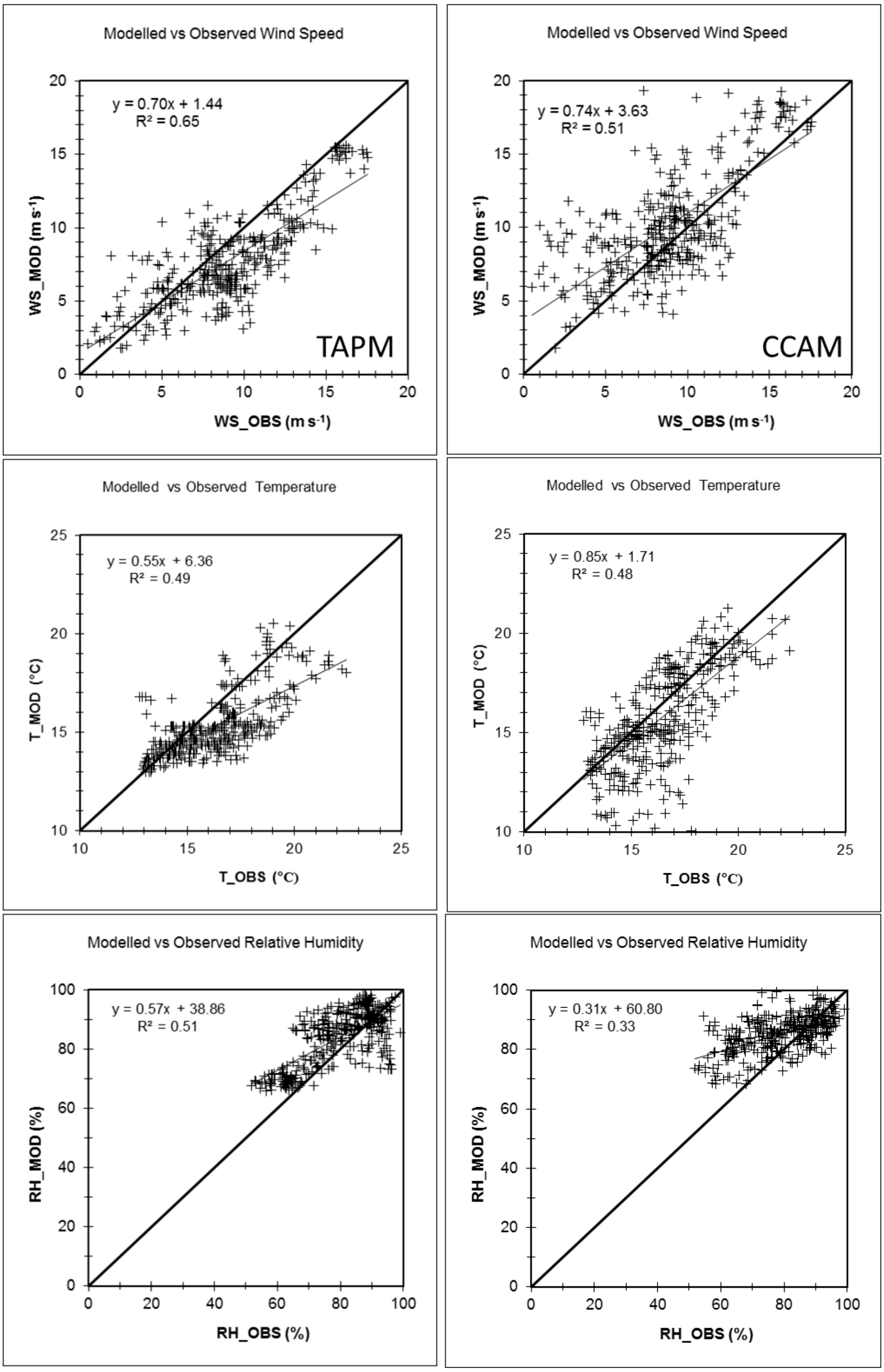

Figure 2. Scatter plots of (by row) observed and modelled 10 m wind speed, screen temperature, relative humidity for (by column). TAPM is shown in the first column and CCAM is shown in the second column.

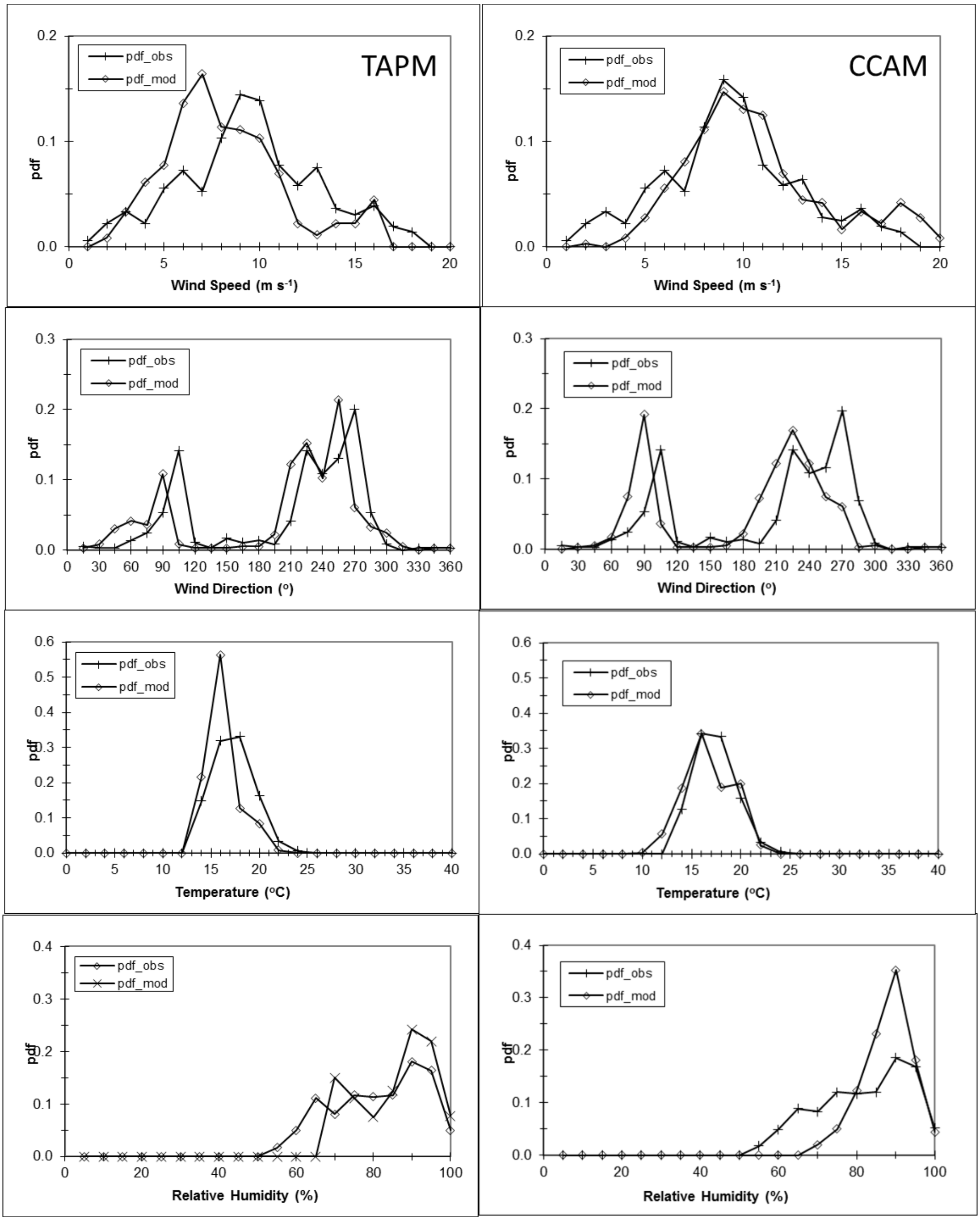

Figure 3. Probability density functions of observed and modelled (by row) 10 m wind speed, 10 m wind direction, screen temperature and screen relative humidity. TAPM results are shown in the first column and CCAM results in the second column.

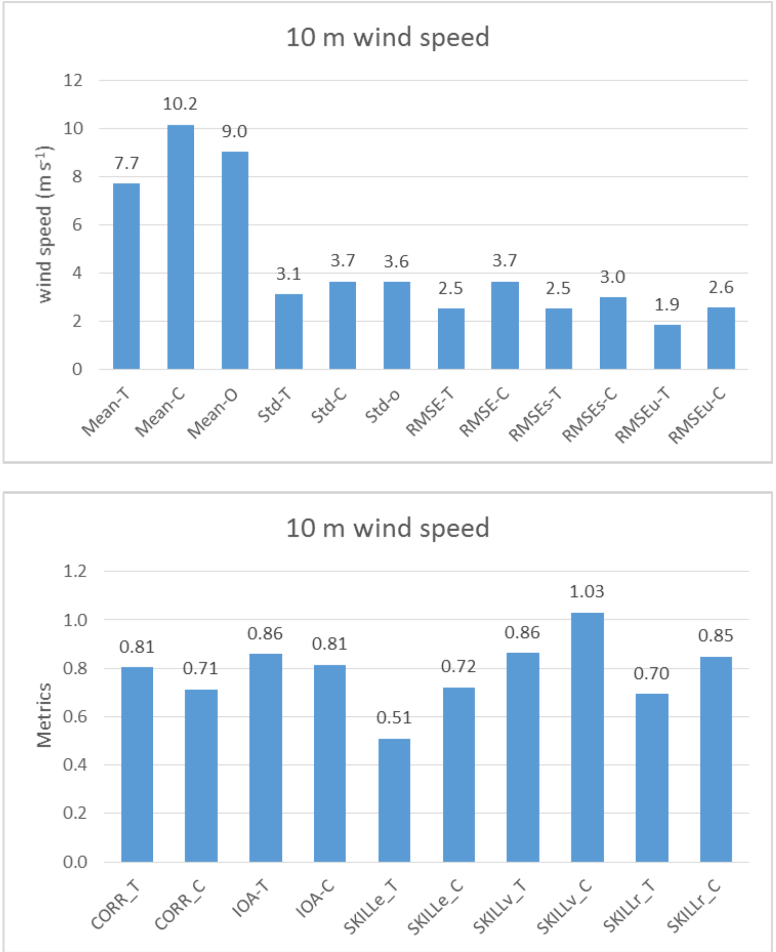

Figure 4. Statistical measures for quantitative comparison of the TAPM and CCAM 10 m wind speed simulations. T=TAPM, C=CCAM, O=Observations. Top- Mean-T, Mean-C, Mean-O; mean TAPM, CCAM and observed 10 m wind speed. Std-T/C standard deviation of the modelled wind (TAPM; CCAM), RMSE- root mean square error; RMSEs- systematic root mean square error; RMSEu- unsystematic root mean square error. Bottom- the metrics are CORR correlation coefficient; IOA- index of agreement; SKILLe = RMSEu/STD-O, SKILLv = Std-model/Std-obs, SKILLr = RMSE/Std-O.

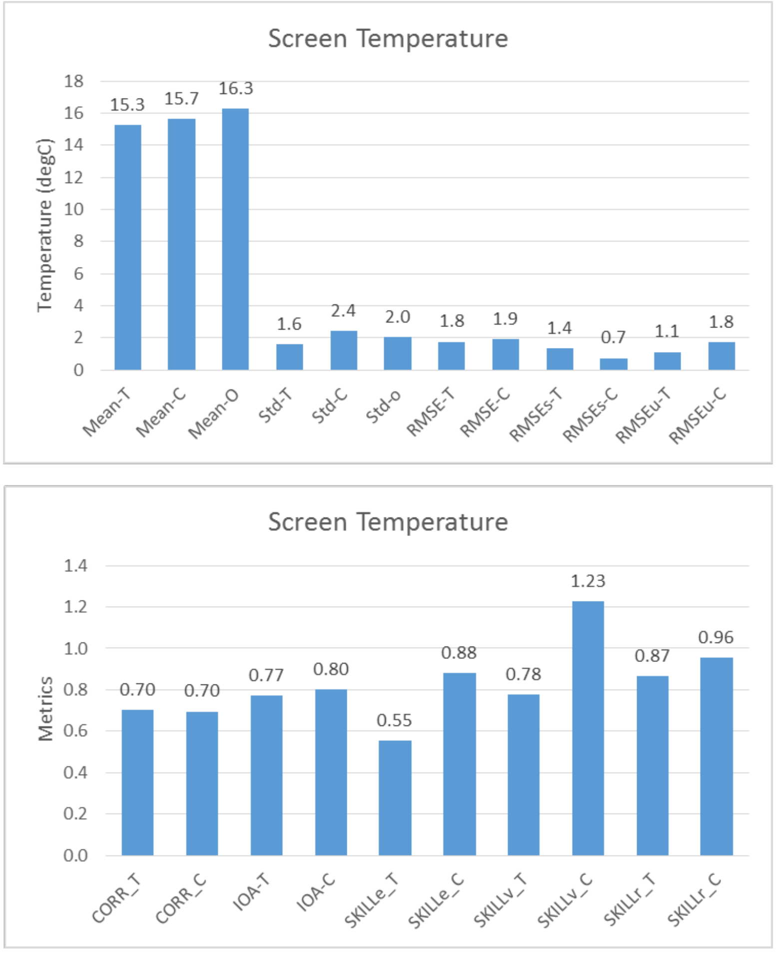

Figure 5. Statistical measures for quantitative comparison of the TAPM and CCAM screen temperature. T=TAPM, C=CCAM, O=Observations. Top- Mean-T, Mean-C, Mean-O; TAPM, CCAM and observed screen temperature. Std-T/C standard deviation of the modelled temperature (TAPM; CCAM), RMSE- root mean square error; RMSEs- systematic root mean square error; RMSEu- unsystematic root mean square error. Bottom- the metrics are CORR correlation coefficient; IOA- index of agreement; SKILLe = RMSEu/STD-O, SKILLv = Std-model/Std-obs, SKILLr = RMSE/Std-O.

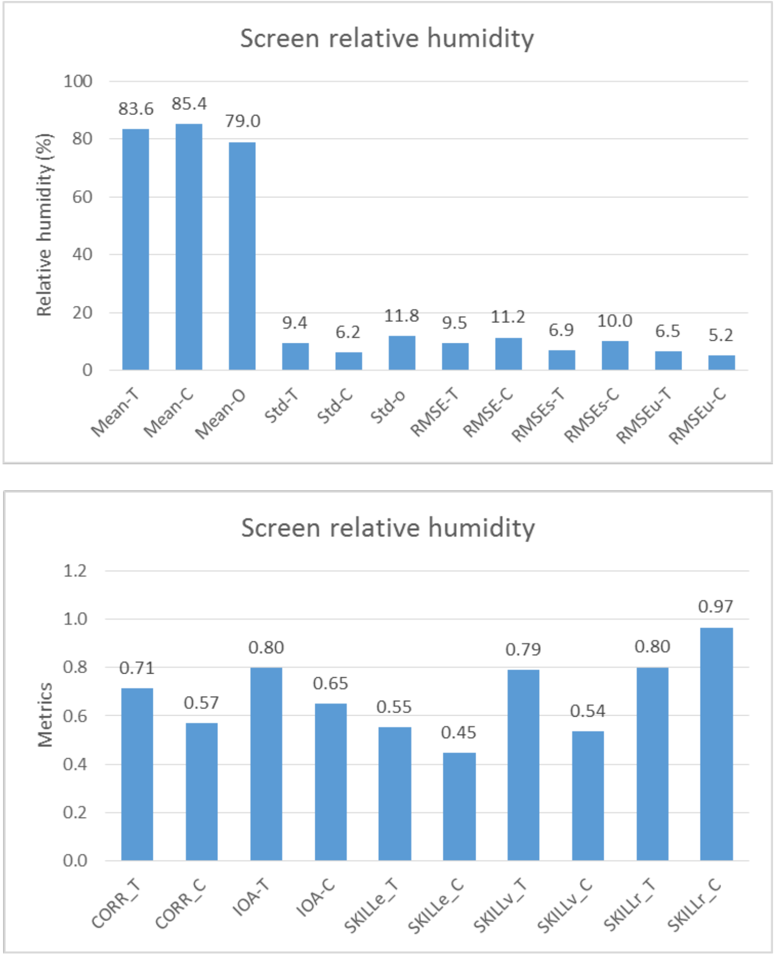

Figure 6. Statistical measures for quantitative comparison of the TAPM and CCAM screen relative humidity. T=TAPM, C=CCAM, O=Observations. Top- Mean-T, Mean-C, Mean-O; mean TAPM, CCAM and observed relative humidity. Std-T/C standard deviation of the modelled relative humidity (TAPM; CCAM), RMSE- root mean square error; RMSEs- systematic root mean square error; RMSEu- unsystematic root mean square error. Bottom- the metrics are CORR correlation coefficient; IOA- index of agreement; SKILLe = RMSEu/STD-O, SKILLv = Std-model/Std-obs, SKILLr = RMSE/Std-O.

Atmospheric soundings were undertaken at least once per day (000 UTC) for the majority of days in the period 8-21 February 2006. Sondes were released from the Cape Grim monitoring station and returned height, pressure, temperature, humidity, wind speed and wind direction data at 10-20 m intervals between the surface and about 3000 m. We have used the data to calculate potential temperature and derived the potential temperature gradient using central differences over height intervals of 30-40 m (to include some smoothing of the raw radiosonde data). The observed boundary layer heights have been diagnosed by searching for positive gradients in the potential temperature profile.

Figure 7 shows the modelled (TAPM and CCAM) hourly PBL time series with the spot hourly PBL observations superimposed on the plot. The figure is helpful because it shows the significantly hourly variability in the modelled PBL- which because Cape Grim is strongly influenced by maritime air, does not strongly follow the typical diurnal variation of PBL growth and collapse associated with sensible heating and long wave radiation cooling over land. Figure 7 suggests that both models have captured important features in the observed PBL heights, including the period of low boundary layer height between hours 168 and 264.

Figure 8 shows a scatter plot of the observed and modelled PBL heights and indicates that 71% of the TAPM PBL heights lie within a factor of two of the observed and 79% of the CCAM PBL heights are within a factor of two. This is a good result given the complexity of the observed meteorological flows at the Cape Grim monitoring station.

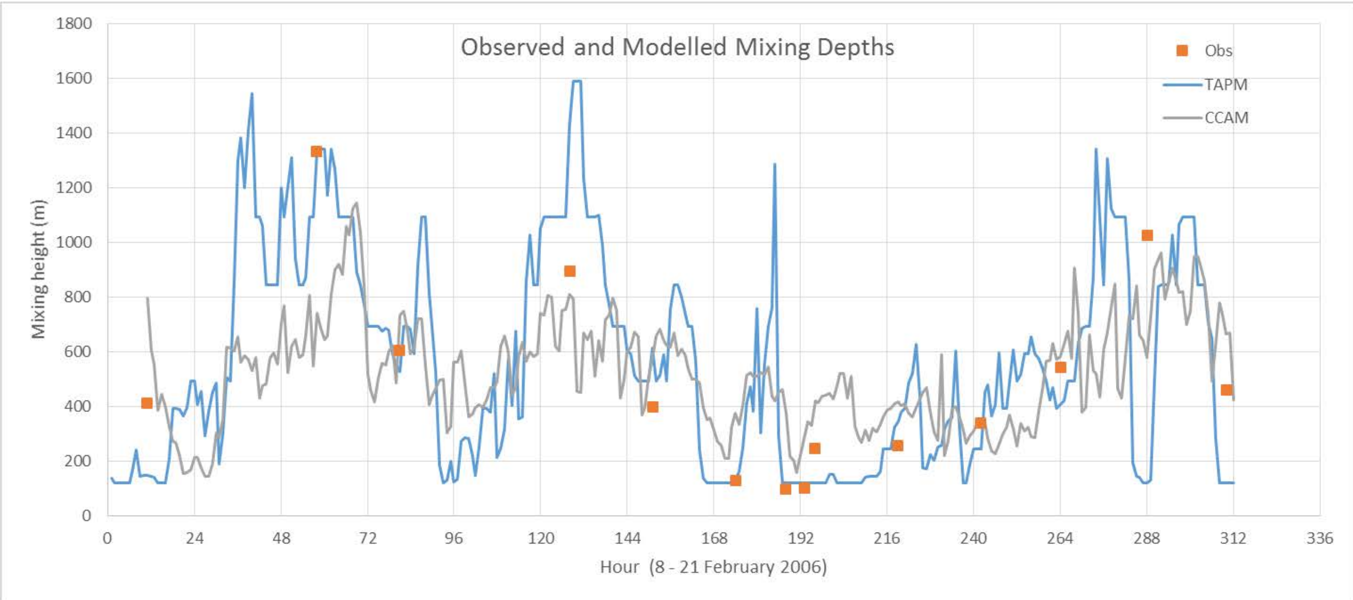

Figure 7. Hourly time series of the modelled (TAPM and CCAM) PBL heights for the period 8 – 21 February 2006. Also shown are PBL heights diagnosed from sonde data released periodically at Cape Grim during the study period.

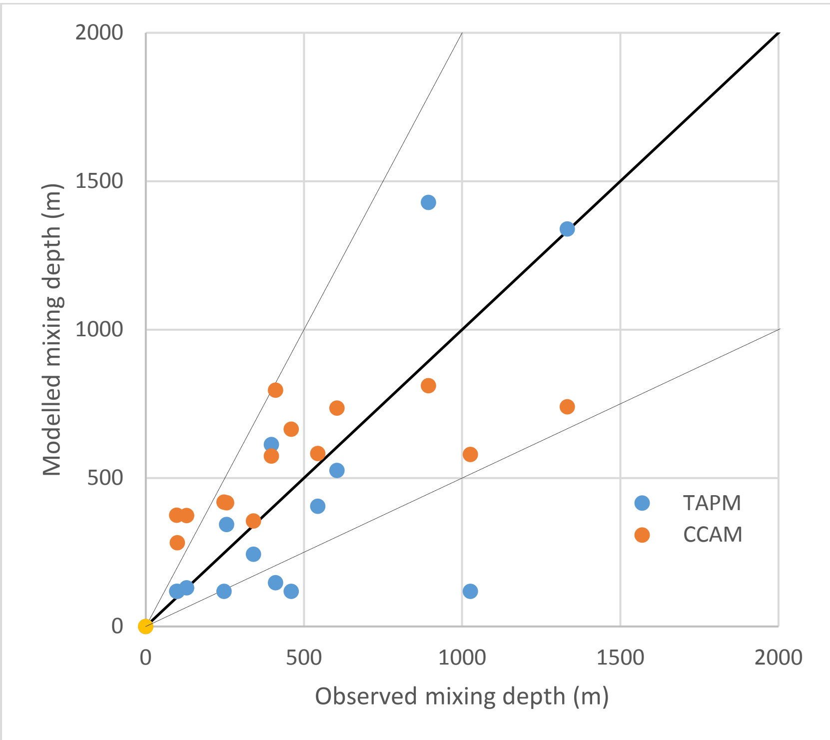

Figure 8. Scatter plot of observed and modelled PBL heights for hours corresponding to sonde releases at Cape Grim in February 2006.

Performance of TAPM-CTM for background O_3

The model generally captures background O_3 very well. The average modelled mean O_3 during background (non BB) periods was 17.7 ppb versus 16.6 ppb observed, with a coefficient of determination of 0.4. The scatter plot below (Figure 9) shows that all modelled concentrations are within a factor of 2 of observations (hourly data). Further, the campaign average diurnal 1 hour O_3 (observed vs modelled) (Figure 10) indicates maximum differences of 2 ppb (< 15% of the hourly mean).

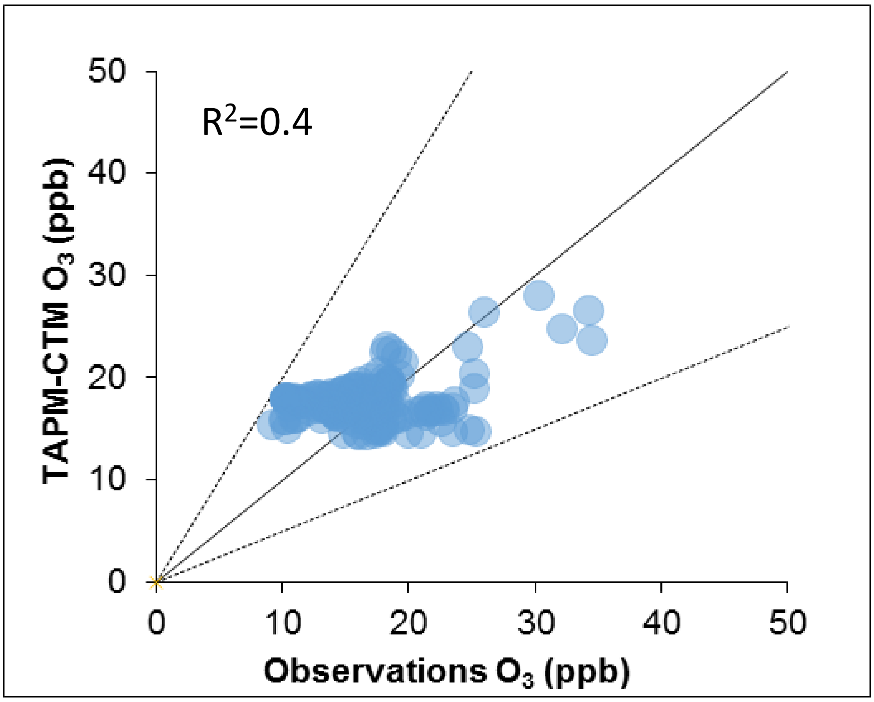

Figure 9. Hourly observed versus modelled O_3 concentrations for background (non-BB) periods

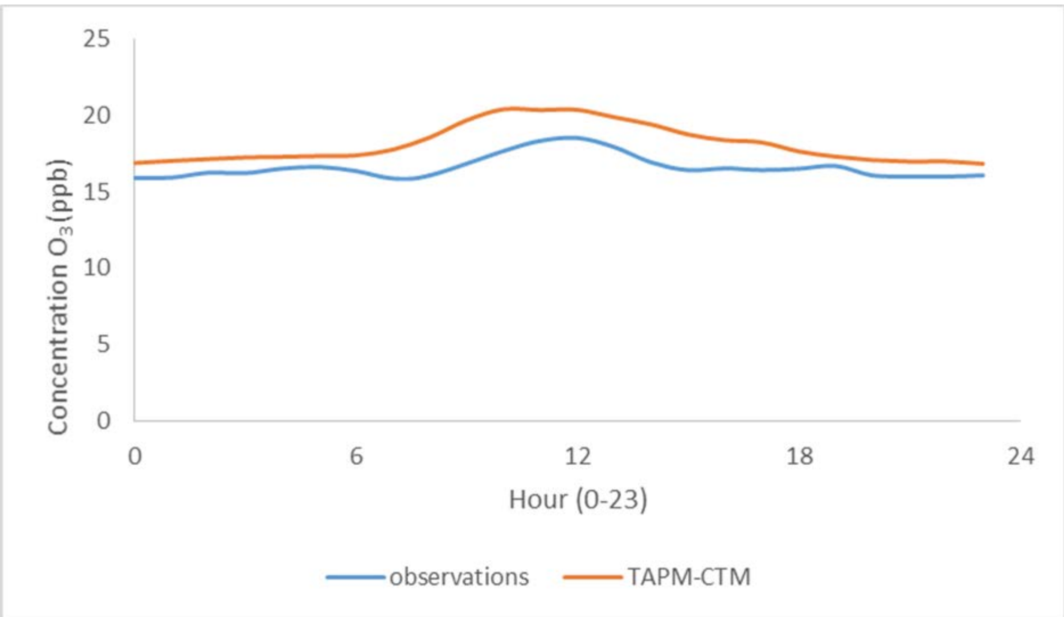

Figure 10. Dirunal observed and modelled (TAPM-CTM) concentration for background (non-BB) periods

Performance of TAPM-CTM and CCAM-CTM for different Emission Factor Scenarios

A series of qualitative and quantitative performance measures have been provided for the different EF scenarios. These measures follow the framework discussed in Dennis et al. (2010), and use the performance goals described in Boylan and Russell (2006). These measures provide quantitative evidence that the best overall agreement with the observations for both primary (EC/CO) and secondary (O_3) species is for the TAPM-CTM run with MCE = 0.89. This is discussed further below, and in the Supplementary material.

Figure 11 shows the quantile–quantile plots of observed and modelled BC/CO for eight model scenarios. For clarity we have plotted the concentration pairs corresponding to each decile in the range 20 to 100%. Note the log scale on both axes. The solid line is 1:1 and the dotted lines delineate a factor of two agreement between observed and modelled BC/CO.

The quantile-quantile plots compare the observed and modelled distributions of BC/CO and are useful for the current morphology where the configuration of a near field source, narrow meandering plume and single receptor make it very challenging for models to simulate the time-and-space coupled behaviour of the in-plume concentrations during plume strikes at the receptor. Additionally, because the modelled and observed concentrations of EC and CO from the fire are a strong function of the plume transport and mixing in addition to the EF, we consider the ratio of BC and CO because ratios of emitted gases and aerosols will be approximately conserved- provided in-plume chemical or physical transformation of these species is not significant, and provided the concentration of each species in the entrained background air is well known.

Figure 11 shows that the BC/CO distributions for each MCE scenario show an approximate linear relationship between the observed and modelled ratios for the first two thirds of each distribution (for BC/CO < 1 ng m^{-3} ppb^{-1}) before the modelled distributions of BC/CO distributions show reduced sensitivity compared to the observed. The TAPM-CTM simulation with MCE=0.89 has the most modelled percentile data points within a factor of two of the observations (6 percentile data points, from 0.3 – 0.8) for BC/CO ratio. The second best agreement with the observations was using CCAM-CTM with MCE = 0.89. Several of the TAPM-CTM and CCAM-CTM model runs overestimated the EC/CO ratio by a factor of up to 8 for MCE=0.95, while the runs with no fire underestimates the observed ratios by a factor of two or larger for the majority of the data points. Overall this indicates that using EF corresponding to an MCE of 0.89 gives the best agreement with the observations for the majority of the BC/CO ratios. Both TAPM-CTM and CCAM-CTM overestimated the ratio at the lowest (0.2 percentile) ratio values, and underestimated the ratio at the highest (1) percentile ratio.

Figure 11 also suggests that the model performance may be limited by the use of a single MCE for a given model scenario with the best model performance at the highest BC/CO being for the MCE=0.95 scenarios, and with the lower MCE scenarios performing better at the lower BC/CO ratios.

Figure 12 and Figure 13 respectively show the mean fractional bias (MFB) and mean fractional error (MFE) of the modelled EC/CO simulations. Following Boylan and Russell (2006) we define MFB and MFE as follows.

$$MFB = 100\% \times \frac{2}{N} \sum \frac{(M_i - O_i)}{(M_i + O_i)}$$

$$MFE = 100\% \times \frac{2}{N} \sum \frac{|M_i - O_i|}{(M_i + O_i)}$$

where M_i and O_i are the ith model–observation concentration pair (here coupled in time and space), and N is the number of data points. Guidance with respect to model performance is given by the criteria (outer lines) and goal (inner lines) which asymptote from a magnitude of 2.0 for EC/CO < 1.0 ng m^{-3} ppb^{-1} to 0.15 and 0.3 (MFB) and 0.35 and 0.5 (MFE) in the limit of large EC/CO (Boylan and Russell, 2006).

Figure 12 shows that the TAPM-CTM; MCE= 0.89 scenario has the smallest MFB, followed by CCAM-CTM; MCE= 0.89. Only the no-fire and MCE= 0.89 scenarios fall within the defined goal. Figure 13 shows the MFE and indicates that all of the simulations are challenged by the defined goal, while only the TAPM-CTM; MCE= 0.89 and the no-smoke scenarios fall within the defined criteria.

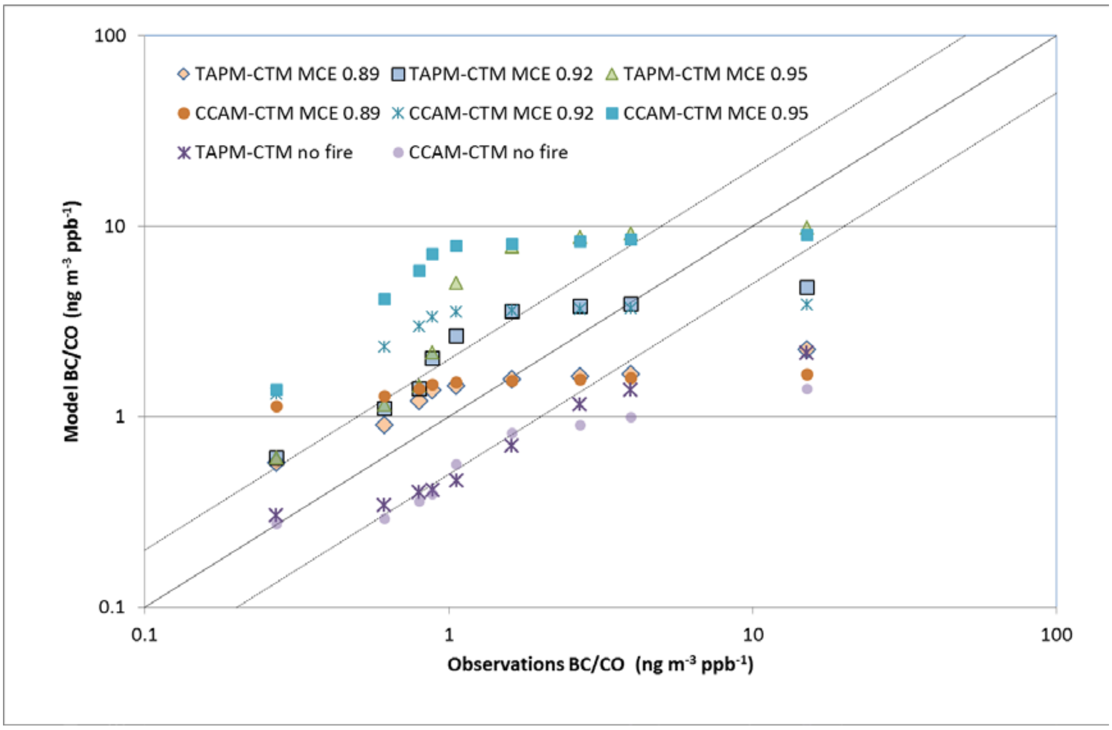

Figure 11. Quantile-quantile plots of observed and modelled BC/CO ratios for the TAPM-CTM and CCAM-CTM simulations. For each scenario, the model-data pairs correspond to the following percentiles- 0.2, 0.3, 0.4, 0.5, 0.6, 0.7, 0.8, 0.9 and 1. Note log scale on both axes. Solid line is 1:1 and dotted lines show performance within a factor of two.

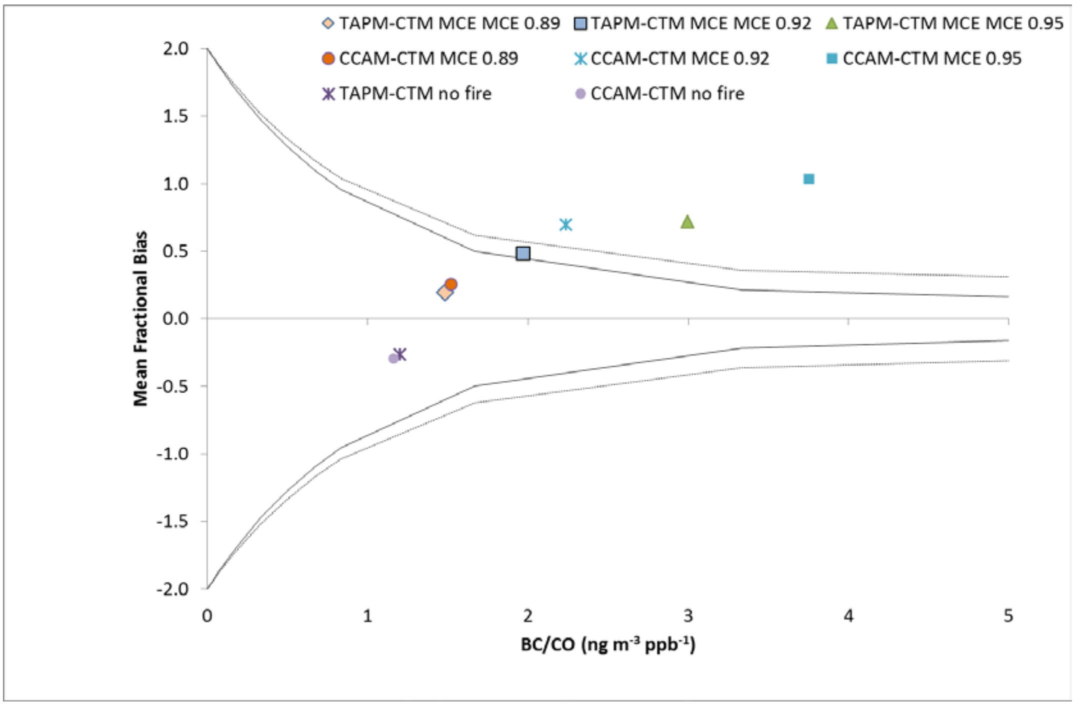

Figure 12. Mean fractional bias for BC/CO. Dotted and solid lines define the performance criteria and goal.

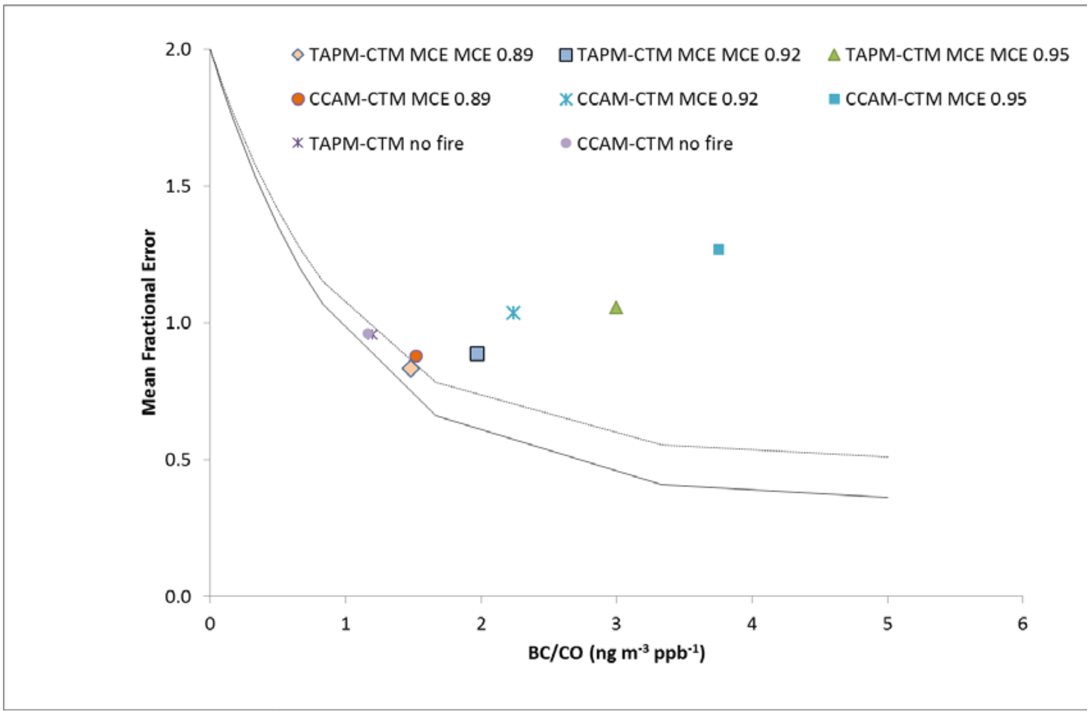

Figure 13. Mean fractional error for BC/CO. Dotted and solid lines define the performance criteria and goal.

With respect to O_3, we analysed the entire data series (both the BB and background periods) because urban air (in non BB periods) represents a significant source of O_3 at Cape Grim, and the test of the models is to reproduce O_3 from fire as well as from other sources.

The quantile-quantile plots in Figure 14 and Figure 15 show that the TAPM-CTM; MCE=0.89 scenario lies close to the 1:1 line for all of the sampled percentiles, and is in best agreement with observations. On the other hand, the MCE=0.92 and MCE=0.95 runs both for TAPM-CTM and CCAM-CTM predict depletion of O_3, an event which is not observed, as discussed in the manuscript. With the exception of these anomalous model depletion events, all modelled percentiles fall well within a factor of two of the observations.

Figure 16 shows the MFB for O_3 and indicates that the lowest MFB was for TAPM-CTM; MCE= 0.92. All but one scenario was able to simulate the one-hour O_3 with a MFB which fell within the range ±0.06. The MFB from all of the simulations fall well within the performance criteria and goal.

Figure 17 shows the MFE for O_3 and indicates that all MFE values are between 0.18- 0.29, again well with the performance criteria and goals. The MFE for TAPM-CTM; MCE=0.89 was 0.2, falling at the lower end of the MFE generating by our suite of simulations.

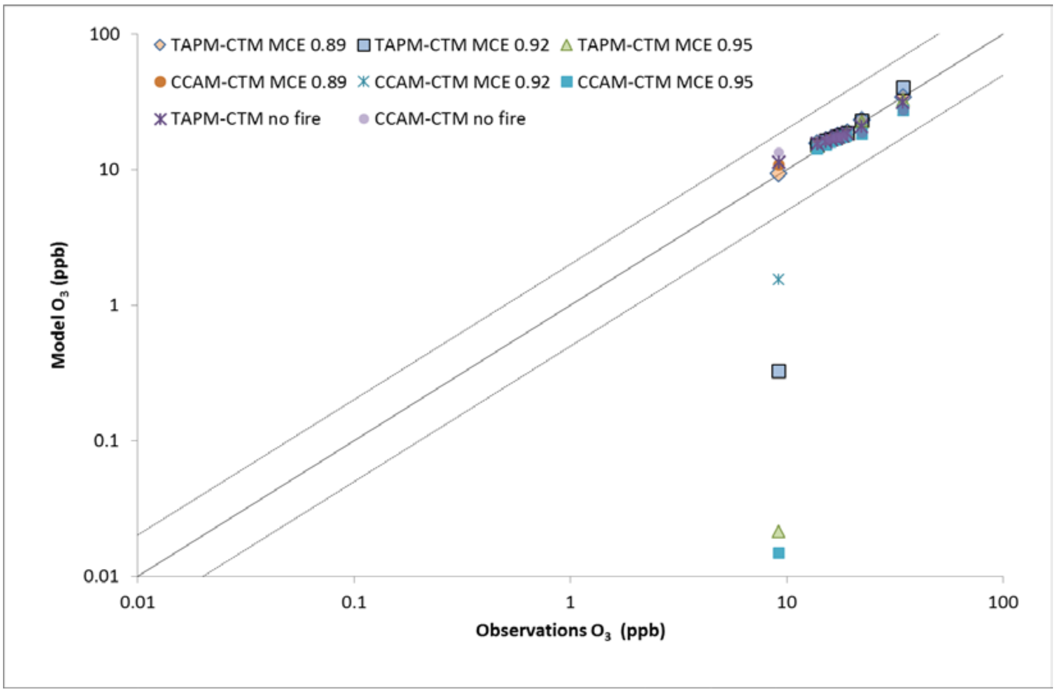

Figure 14. Quantile-quantile plots of observed and modelled O_3 for the TAPM-CTM and CCAM-CTM simulations. For each scenario, the model-data pairs correspond to the following percentiles- 0.2, 0.3, 0.4, 0.5, 0.6, 0.7, 0.8, 0.9 and 1. Note log scale on both axes. Solid line is 1:1 and dotted lines show performance within a factor of two.

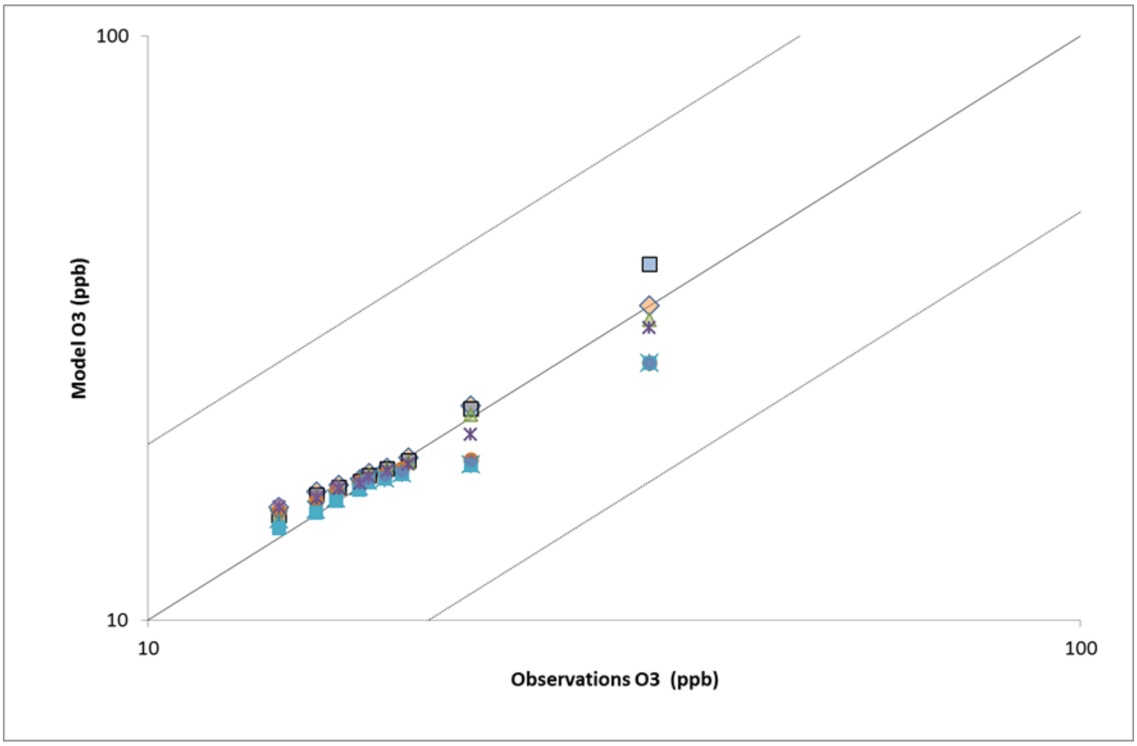

Figure 15. Quantile-quantile plots of observed and modelled O_3 for the TAPM-CTM and CCAM-CTM simulations. The plot is similar to Figure 14 above but with smaller concentration range so detail can be seen.

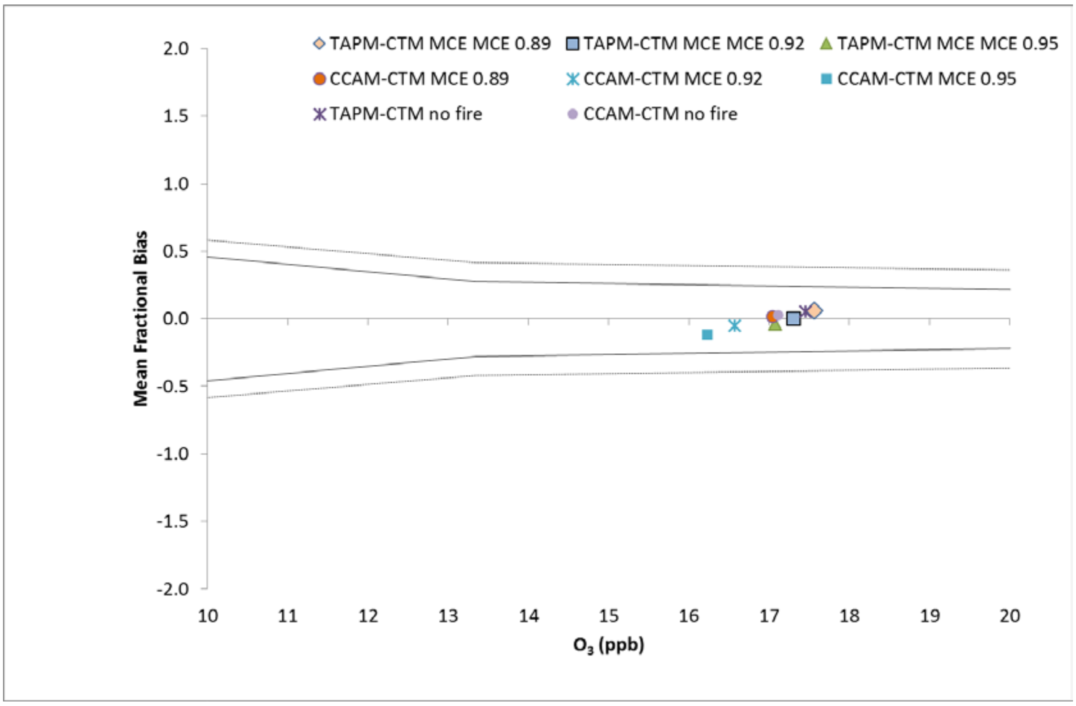

Figure 16 . Mean fractional bias for O_3. The dotted and solid lines define the performance criteria and goal.

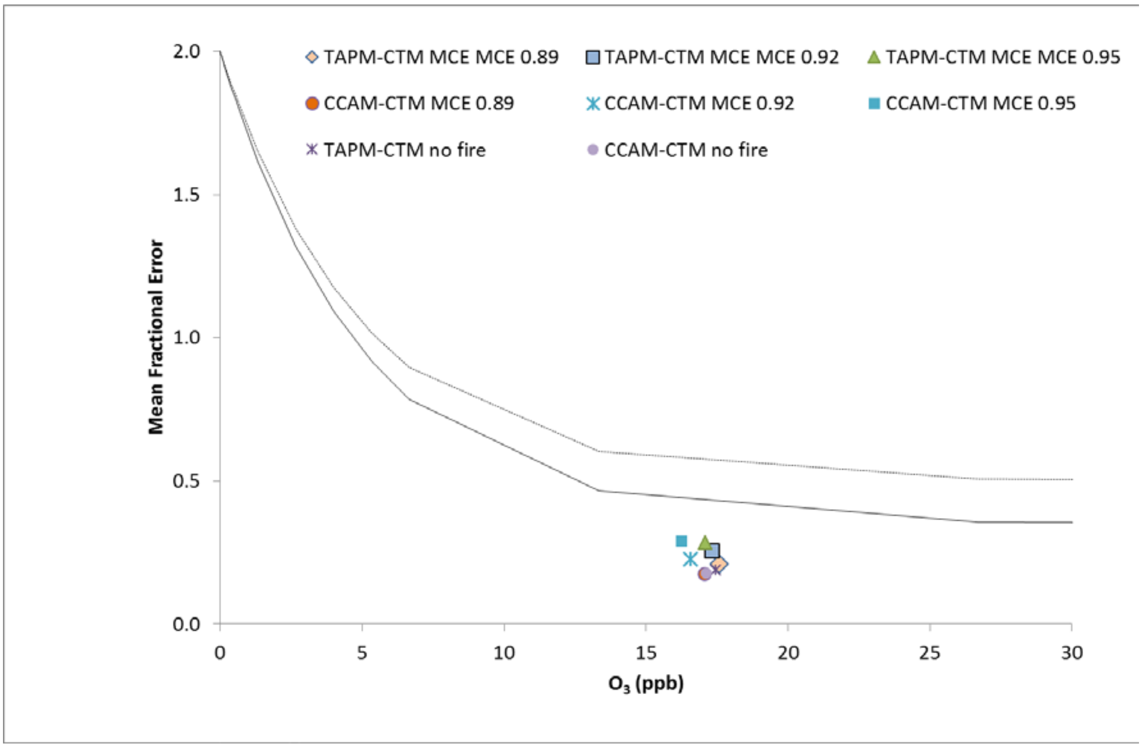

Figure 17. Mean fractional error for O_3. The dotted and solid lines define the performance criteria and goal.

In summary, the quantile-quantile plots for EC/CO (fire periods) and O_3 (all periods) demonstrate that, generally, the TAPM-CTM MCE=0.89 scenario is in best agreement with observations. This scenario also has the lowest MFB and MFE for EC/CO, and small values of MFB and MFE for O_3 which fall well within our performance criteria and goals. Additionally, this scenario did not generate the anomalous depletion of O_3 as modelled by the MCE=0.92 and MCE=0.95 scenarios.

Performance of TAPM-CTM and CCAM-CTM for BB2

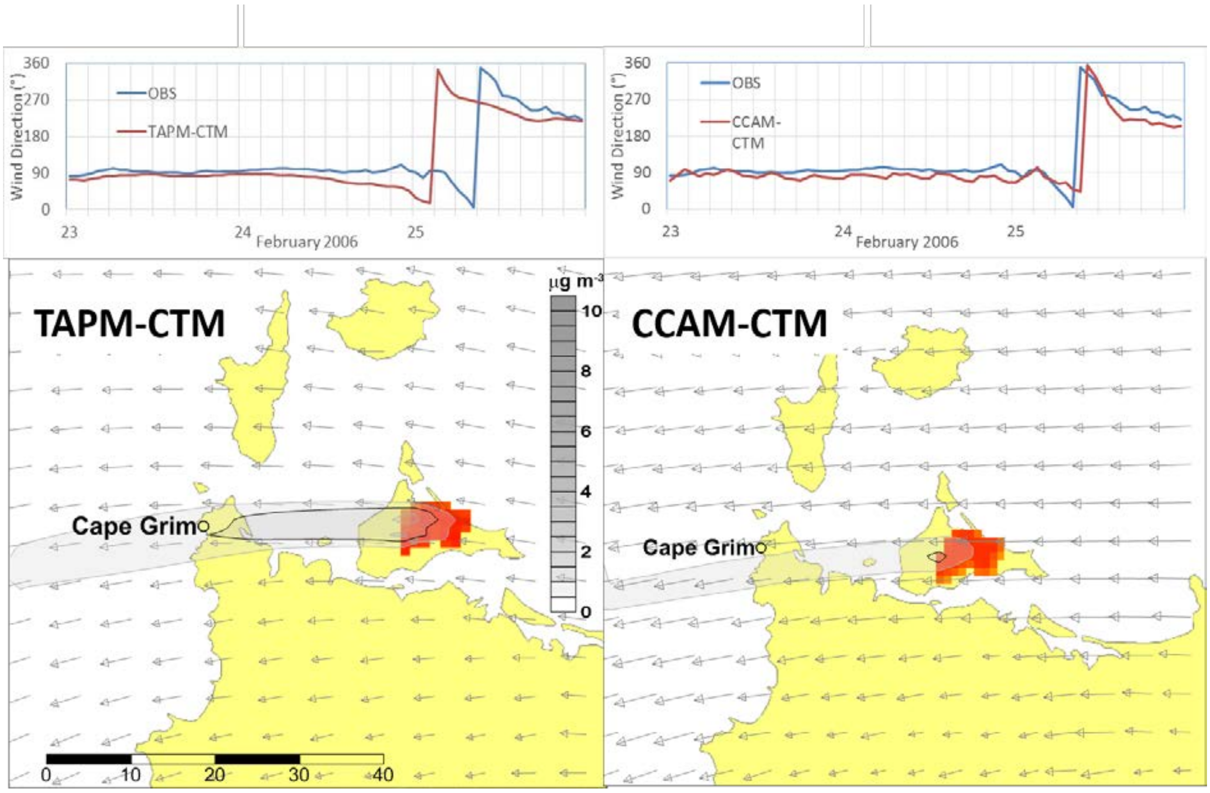

Figure 18. Wind direction and EC concentrations for TAPM-CTM and CCAM-CTM at 05:00 on the 24 February during BB2.

Model output of TAPM-CTM and CCAM-CTM during BB1 as discussed in Section 3.1 of the manuscript

References

Hurley, P., 2008. Development and verification of TAPM. Nato Sci Peace Secur, 208-216.

Hurley, P.J., Physick, W.L., Luhar, A.K., Edwards, M., 2005. The air pollution model (TAPM) version 3. Part 2, Summary of some verification studies. . CSIRO, CSIRO Atmospheric Research, Aspendale, Victoria 3195 Australia.

McGregor, J.L., Dix, M.R., 2008. An updated description of the Conformal-Cubic atmospheric model. High Resolution Numerical Modelling of the Atmosphere and Ocean, 51-75.

Thorpe, A.J., 1985. Mesoscale Meteorological Modelling By R. A. Pielke. Academic Press, 1984, Pp. 612, £55.50, US$79. Q J Roy Meteor Soc 111, 671-672.

Willmott, C.J., 1981. ON THE VALIDATION OF MODELS. Physical Geography 2, 184-194.

Akagi, S.K., Yokelson, R.J., Wiedinmyer, C., Alvarado, M.J., Reid, J.S., Karl, T., Crounse, J.D., Wennberg, P.O., 2011. Emission factors for open and domestic biomass burning for use in atmospheric models. Atmospheric Chemistry and Physics 11, 4039-4072.

Boylan, J.W., Russell, A.G., 2006. PM and light extinction model performance metrics, goals, and criteria for three-dimensional air quality models. Atmospheric Environment 40, 4946-4959.

Castellanos, P., Boersma, K.F., van der Werf, G.R., 2014. Satellite observations indicate substantial spatiotemporal variability in biomass burning NOx emission factors for South America. Atmospheric Chemistry and Physics 14, 3929-3943.

Dennis, R., Fox, T., Fuentes, M., Gilliland, A., Hanna, S., Hogrefe, C., Irwin, J., Rao, S.T., Scheffe, R., Schere, K., Steyn, D., Venkatram, A., 2010. A framework for evaluating regional-scale numerical photochemical modeling systems. Environ Fluid Mech 10, 471-489.

Finch, D.P., Palmer, P.I., Parrington, M., 2014. Origin, variability and age of biomass burning plumes intercepted during BORTAS-B. Atmos. Chem. Phys. 14, 13789-13800.

Galbally, I.E., Meyer, C.P., Bentley, S.T., Lawson, S.J., Baly, S.B., 2007. Reactive gases in near surface air at Cape Grim, 2005-2006 – I E Galbally, C P Meyer, S T Bentley. Baseline Atmospheric Program Australia 2005-2006, 77-79.

Gras, J.L., 2007. Particles Program Report. Baseline Atmospheric Program Australia 2005-2006, 85-86.

Hurley, P., 2008. Development and verification of TAPM. Nato Sci Peace Secur, 208-216.

Hurley, P.J., Physick, W.L., Luhar, A.K., Edwards, M., 2005. The air pollution model (TAPM) version 3. Part 2, Summary of some verification studies. . CSIRO, CSIRO Atmospheric Research, Aspendale, Victoria 3195 Australia.

Korontzi, S., Ward, D.E., Susott, R.A., Yokelson, R.J., Justice, C.O., Hobbs, P.V., Smithwick, E.A.H., Hao, W.M., 2003. Seasonal variation and ecosystem dependence of emission factors for selected trace gases and PM2.5 for southern African savanna fires. Journal of Geophysical Research: Atmospheres 108, n/a-n/a.

Krummel, P.B., Fraser, P., Steele, L.P., Porter, L.W., Derek, N., Rickard, C., Dunse, B.L., Langenfelds, R.L., Miller, B.R., Baly, S.B., McEwan, S., 2007. The AGAGE in situ program for non-CO2 greenhouse gases at Cape Grim, 2005-2006: methane, nitrous oxide, carbon monoxide, hydrogen, CFCs, HCFCs, HFCs, PFCs, halons, chlorocarbons, hydrocarbons and sulphur hexafluoride. Baseline Atmospheric Program Australia 2005-2006.

Lawson, S. J., Keywood, M. D., Galbally, I. E., Gras, J. L., Cainey, J. M., Cope, M. E., Krummel, P. B., Fraser, P. J., Steele, L. P., Bentley, S. T., Meyer, C. P., Ristovski, Z., and Goldstein, A. H.: Biomass burning emissions of trace gases and particles in marine air at Cape Grim, Tasmania, Atmos. Chem. Phys., 15, 13393-13411, 10.5194/acp-15-13393-2015, 2015.

McGregor, J.L., Dix, M.R., 2008. An updated description of the Conformal-Cubic atmospheric model. High Resolution Numerical Modelling of the Atmosphere and Ocean, 51-75.

Thorpe, A.J., 1985. Mesoscale Meteorological Modelling By R. A. Pielke. Academic Press, 1984, Pp. 612, £55.50, US$79. Q J Roy Meteor Soc 111, 671-672.

Urbanski, S.P., 2013. Combustion efficiency and emission factors for wildfire-season fires in mixed conifer forests of the northern Rocky Mountains, US. Atmos. Chem. Phys. 13, 7241-7262.

van Leeuwen, T.T., Peters, W., Krol, M.C., van der Werf, G.R., 2013. Dynamic biomass burning emission factors and their impact on atmospheric CO mixing ratios. Journal of Geophysical Research-Atmospheres 118, 6797-6815.

Willmott, C.J., 1981. ON THE VALIDATION OF MODELS. Physical Geography 2, 184-194.